computation

MDPI

Article

Finite Element Analysis of ACL Reconstruction-Compatible Knee Implant Design with Bone Graft Component

Ferdinand Lauren F. Carpena [1,2] and Lemmuel L. Tayo [2,3,*]

[1] School of Mechanical and Manufacturing Engineering, Mapúa University, Manila 1002, Philippines; laurencarpena@gmail.com
[2] School of Chemical, Biological, and Materials Engineering and Sciences, Mapúa University, Manila 1002, Philippines
[3] Department of Biology, School of Medicine and Health Sciences, Mapúa University, Makati 1200, Philippines
* Correspondence: lltayo@mapua.edu.ph

Abstract: Knee osteoarthritis is a musculoskeletal defect specific to the soft tissues in the knee joint and is a degenerative disease that affects millions of people. Although drug intake can slow down progression, total knee arthroplasty has been the gold standard for the treatment of this disease. This surgical procedure involves replacing the tibiofemoral joint with an implant. The most common implants used for this require the removal of either the anterior cruciate ligament (ACL) alone or both cruciate ligaments which alters the native knee joint mechanics. Bi-cruciate-retaining implants have been developed but not frequently used due to the complexity of the procedure and the occurrences of intraoperative failures such as ACL and tibial eminence rupture. In this study, a knee joint implant was modified to have a bone graft that should aid in ACL reconstruction. The mechanical behavior of the bone graft was studied through finite element analysis (FEA). The results show that the peak Christensen safety factor for cortical bone is 0.021 while the maximum shear stress of the cancellous bone is 3 MPa which signifies that the cancellous bone could fail when subjected to the ACL loads, depending on the graft shear strength which could vary depending on the graft source, while cortical bone could withstand the walking load. It would be necessary to optimize the bone graft geometry for stress distribution as well as to evaluate the effectiveness of bone healing prior to implementation.

Keywords: total knee replacement; ACL reconstruction; ACL graft; bone graft; finite element analysis

check for updates

Citation: Carpena, F.L.F.; Tayo, L.L. Finite Element Analysis of ACL Reconstruction-Compatible Knee Implant Design with Bone Graft Component. *Computation* **2023**, *11*, 151. https://doi.org/10.3390/computation11080151

Academic Editor: Yudong Zhang

Received: 27 June 2023
Revised: 22 July 2023
Accepted: 1 August 2023
Published: 2 August 2023

Copyright: © 2023 by the authors. Licensee MDPI, Basel, Switzerland. This article is an open access article distributed under the terms and conditions of the Creative Commons Attribution (CC BY) license (https://creativecommons.org/licenses/by/4.0/).

1. Introduction

The musculoskeletal system enables different movements in other parts of the body as well as stability. It comprises muscle groups, tendons, structures made of connective tissues such as bones and joints, and soft tissues like cartilage and ligaments [1]. These individual parts work in proper coordination to create safe musculoskeletal movement and promote biomechanical stability in the human body. Decreased injury rates have been observed in programs that focus on the stability of the lower body [2].

The joint of the lower body that is most susceptible to instability is the tibiofemoral joint or the knee since it carries the upper body weight, allows the limbs to create a walking cycle, and absorbs and distributes impact loads when walking or jumping as transferred by the tibia [3]. Because of the different loads as well as the continuous changes in the loading condition of the knee joint during normal gait and other daily activities, the interface of the knee can eventually wear out. Knee osteoarthritis is a progressive condition where the shock-absorbing portion of the knee called the articular cartilage and meniscus becomes damaged and starts to degenerate until it becomes a disability [4]. Considered as a degenerative disease, there is a point where medications and supplements cannot reverse the damage to these soft tissues and patients eventually resort to total knee arthroplasty in later stages [5]. Knee arthroplasty or total knee replacement involves replacing the tibiofemoral joint interface, which includes the articular cartilages and meniscus, with a

synthetic implant [6]. But using this method, the most used implant designs require the removal of either the anterior cruciate ligament (ACL) only or both cruciate ligaments [7]. This is where gait problems could arise since the native structure of the joint is lost.

The ACL is responsible for limiting the movement of the tibia towards the front of the femur which therefore prevents overextension of the knee [8]. When this ligament is removed, instability on the knee may be observed as rotation on the joint can increase and the tibia may translate over the femur onto the knee joint. The ACL is one of the most focused subjects of research when it comes to structures in the human body [9]. The huge volume of studies related to this have provided adequate amounts of information regarding the biomechanics of the structure as well as biological data involved in ACL tears. The current standard in the treatment of these tears is through ACL reconstruction where a graft from the hamstring tendons replaces the torn ligament through surgery [10]. In this method, the graft serves as a scaffold as well as the source of tissues that should be incorporated into the bones. But there are existing issues regarding the postoperation effects and after rehabilitation. The complications that could arise with this treatment include improper positioning, fractures of the patella, stiffness, and common infection [11].

The use of prostheses is very common in medical applications as it provides better solutions to physical problems in the body and orthopedics is one field that takes advantage of this. Multiple prosthetic devices have been used by people both for lower limb and upper limb applications [12]. One of the most common prostheses is a knee implant for the treatment of knee osteoarthritis. Most of the available knee implants require the removal of both cruciate ligaments or leaving the posterior cruciate ligament attached, but studies show that better gait and knee functionalities are present when the ACL is retained [13]. Bi-cruciate retaining knee implants have been developed to leave both cruciate ligaments intact but the complexity of this makes the option difficult. Some of the intraoperative complications with this type of implant are the breakage of the tibial eminence as well as rupture of the ACL, which leads to either reconstruction of the ACL or the removal of this ligament and choosing a different implant design [14]. Especially with a torn ACL, a more complex approach must be conducted to achieve success in both ACL reconstruction and total knee arthroplasty.

For ACL reconstruction performed on the knee using the surgical replacement approach, there would be insufficient area for the ACL to heal and grow in its original attachment area. For the ACL graft to heal appropriately, the surrounding area should provide suitable conditions for proper attachment so growth and remodeling can be initiated. Bone grafts have been used to treat structural defects as they are capable of bone-to-bone or bone-like structure incorporation [15]. Cortical bone grafts can sustain large loads, but cancellous bone grafts promote faster healing but with less load capacity [16]. It is important to find the fine line that suits the required loading condition and bone incorporation. A stress analysis can provide insight into the structural integrity of a material under given loading conditions [17]. This could be used to identify the outcomes when a bone graft is situated in specific loads.

This study aimed to generate a tibiofemoral joint model with a knee implant designed to have a bone graft that can sustain the ACL mechanics of the joint when ACL reconstruction is conducted and analyze the capability of the bone graft to withstand the knee loads and ACL loads using FEBio Studio to conduct a finite element analysis (FEA).

This study would be beneficial in the development of patient-specific knee implants in specific cases where the ACL is torn by considering the incorporation of a bone graft into the implant. Data from this could also be utilized in future studies on both bi-cruciate knee implants and ACL reconstruction. This could provide better options for patients without considering the risk of losing some functionality in their injured knee by having an intact ACL after a knee replacement.

The study was limited to the analysis of the bone graft for the knee joint model. The FEA only revolves around the ACL graft, femoral and tibial components of the knee implant, and bone graft. This does not include the patellar component of the knee implant. The

study was also bounded by the constraints of the dataset geometries such that validation could still be conducted. The considerations of the reconstructed ACL were not included in the analysis to simplify the model and focus on the implant stresses. In addition to this, the analysis only pertains to the situation of the bone graft before bone incorporation and healing.

2. Materials and Methods

2.1. Preparation of Knee Implant and Ligament Graft Geometries

The general workflow for the creation of the knee implant was based on the literature [18]. Computer tomography datasets of knees were obtained from SimTK's 6th Grand Challenge Competition (6th GCC) [19]. The CT images before implantation were segmented and reconstructed to create a refined model of the tibia and femur using an open source segmentation tool called 3D Slicer [20]. The dataset also provided the femoral component, tibial insert, tibial tray, femur, tibia, and fibula geometries of the patient. The geometries were initially not aligned which required a basis for alignment. This was achieved by segmenting CT images of the knee postimplantation to obtain the actual position of the knee implants as well as the position of the femur, tibia and fibula. Because the tibiofemoral joint of the postimplantation was too cloudy due to the presence of the metal, the segmented femur, tibia, and fibula were aligned first to the segmented bones postimplantation. When the actual positions for the three bones were obtained, the geometries from the dataset were then aligned with bones on the actual positions. All of these were conducted in 3D Slicer using fiducial registration where specific landmarks are registered to match the same landmarks on the other geometries. The tibial tray and tibial insert (cruciate-retaining implant) geometry were modified in Fusion 360 version 2.0.15995 by creating a cylindrical hole on the two components which served as the tibial tunnel bone graft for the ACL graft. The locations of the insertion tunnels on the tibial and femoral components were determined as mentioned in the literature [21]. The angle of the tunnels was set according to the process and data from the literature [22]. The femur and the femoral component were rotated to 30 degrees in the X direction to mimic the initial position of ACL reconstruction which can be seen in Figure 1, where the components such as the tibia (brown), fibula (blue-green), femur (peach), tibial tray (cyan), tibial insert (purple), femoral component (yellow), ACL graft (blue), and bone graft (orange) are shown. A single reference point was used as the joint axis which was based on the description of Yin et al. (2015) [23].

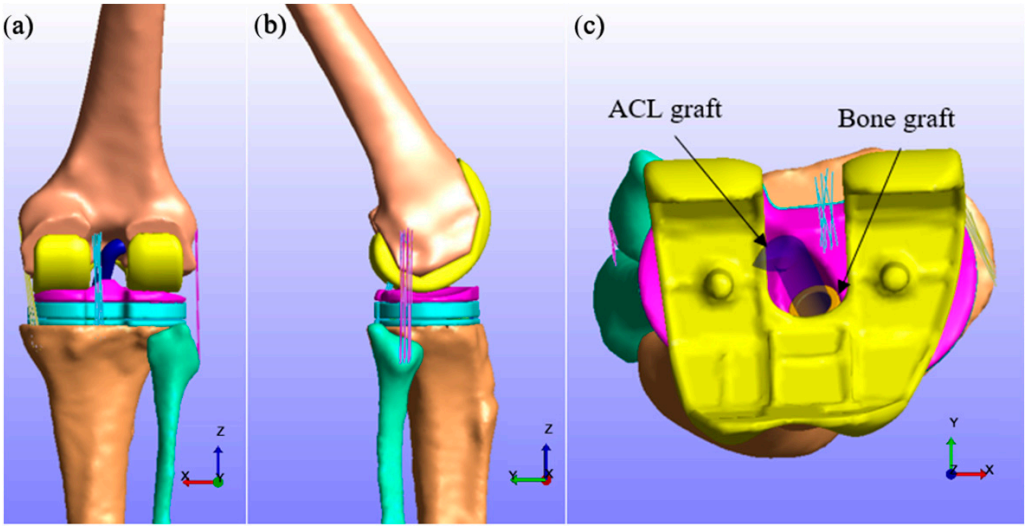

Figure 1. Knee joint assembly viewed at the (**a**) coronal plane, (**b**) sagittal plane, and (**c**) axial plane (without the femur).

For the ligament, a cylindrical structure was used to represent the graft geometry since ACL grafts are shaped into a cylinder during preparation for surgery. The diameter of the ligament was set to 8.5 mm. This was based on the optimal ACL graft diameter as mentioned in the literature [24].

The bone graft that holds the ACL graft was also a cylinder with an inner tunnel. The inner diameter was the ACL graft diameter, and the thickness was based on the range of the surface area of cadaveric ACL-tibial attachment with reference to the study of Tran and Tran (2018) and the geometry of the tibial insert [25]. This bone graft was inclined such that it had the optimal tunnel angle based on the literature and the effect on the geometry of the tibial insert [22]. The chosen tunnel angles were 50 degrees on the sagittal plane and 70 degrees on the coronal plane.

2.2. Finite Element Modelling in FEBio

The assembly of the geometries was imported into FEBio. The tibia and femur were modeled as rigid structures like most ACLR studies that focus on the ligaments [26]. Ti6Al4V was used as the material for the tibial tray in the form of a rigid body, CoCrMo alloy was used for the femoral component, which was modeled as neo-Hookean, while the tibial insert was made up of ultrahigh molecular weight polyethylene. The Poisson's ratio for titanium material, CoCrMo, and bone was 0.3. The elastic modulus was 110 GPa for the Ti6Al4V, 210 GPa for the CoCrMo, and 13.4 GPa for the bone. The tibial insert was also modeled as a neo-Hookean material with a Young's modulus and Poisson's ratio of 1200 MPa and 0.46, respectively. The bone graft was set to have two types of material, cancellous and cortical bone for comparison. The Poisson's ratio for materials was 0.3 and Young's modulus was set to 400 MPa and 17 GPa for the cancellous and cortical bones, respectively [27]. The modeling of the ACL graft differs in the literature, but for this study, the hyperelastic model was used. Hyperelastic models are capable of undergoing large reversible deformations which linear models cannot achieve and this makes for a better fit to the biomechanical structures such as the ACL [28]. An uncoupled transversely isotropic Mooney–Rivlin model was used for the ACL graft with properties for quadruple semitendinosus graft from the literature [26]. To minimize the number of nodes in the models, the elements used for the meshing were four-node tetrahedral. These properties can be seen in Table 1.

Table 1. Material properties and mesh elements of each model component.

Model Part	Properties	Mesh Elements
Femur, tibia, and fibula [18]	E = 13.4 GPa ν = 0.24	90,136
CoCrMo [18]	E = 210 GPa ν = 0.3	54,921
UHMWPE [18]	E = 1.2 GPa ν = 0.46	14,692
Ti6Al4V alloy [18]	E = 110 GPa ν = 0.3	37,146
Cortical bone [27]	E = 17 GPa ν = 0.3	28,103
Cancellous bone [27]	E = 0.4 GPa ν = 0.46	28,103
ACL graft [26]	c1 = 2.75 c2 = 0.065 c3 = 115.89 c4 = 512.73 λ = 1.042	34,381

2.3. Defining Loads and Boundary Conditions

To mimic the knee joint motion, three rigid cylindrical connectors were created for the three axes. X and Y translations were fixed as well as the Z rotation for the femur, similar to the knee model in the literature to increase the chances for convergence and minimize terminations of the simulation due to the complexity of the model [18]. The rigid cylindrical connector for the X rotation was responsible for the knee flexion angles, and this connected the rigid femur with an imaginary rigid body. The Y rigid cylindrical connector was intended for abduction and adduction movements, and it connected the first imaginary rigid body to a second imaginary rigid body. The Z rigid cylindrical connector was responsible for the vertical translation of the loads, and connected the second imaginary rigid body and the tibia. Here, the tibial tray, tibia, and fibula were all fixed in place to ensure convergence and this can be seen in Figure 2. Rigid contact was defined between the femoral component and femur, tibial tray and tibial insert, ACL graft and both femur and tibia. Sliding elastic contact was used in between the tibial insert and femoral component, bone graft and tibial insert, and the ACL graft and bone graft.

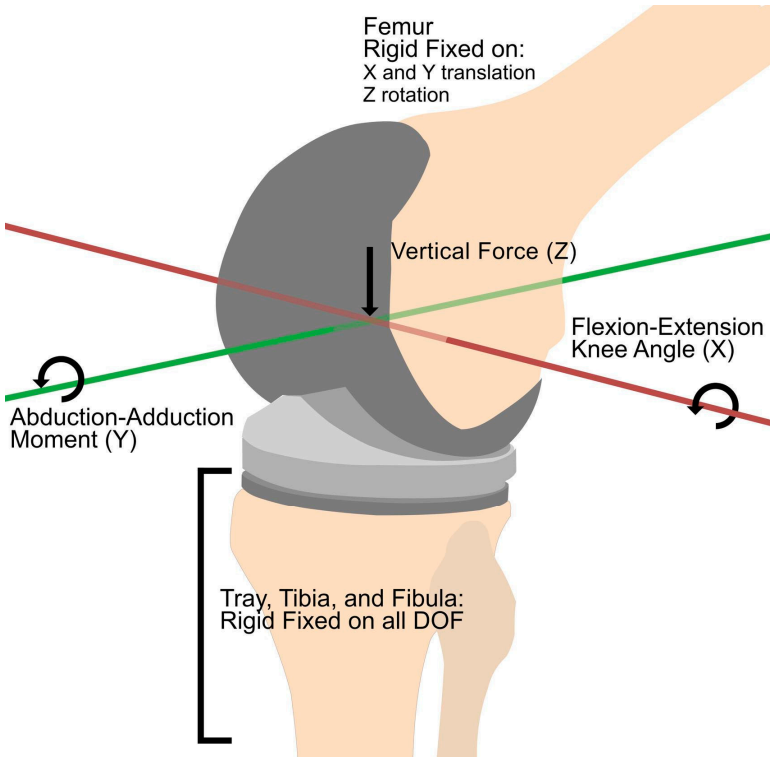

Figure 2. Loading diagram of the knee joint model.

In order to obtain data that represented a wider range of knee loads, standardized loads were used based on Bergmann et al.'s study [29]. The load curve of the tibiofemoral joint at the Z axis was prescribed on the Z rigid connector, the moment curve for the Y rigid connector, and knee flexion angles for the X rigid connector, throughout a single walking cycle. An initial vertical translation was also prescribed until contact on the joint was obtained. A dynamic simulation was conducted and from this, the results were analyzed.

3. Results

3.1. Comparison of Contact Knee Loads

In simulating knee mechanics, knee load is one of the parameters that is commonly observed and considered. Contact knee loads refer to the loads induced in the tibiofemoral interface due to the contact between the femur and the tibial plateau for a normal knee, and the femoral component and tibial insert. Biomechanical simulation of the knee joint is seen to be a more economical way to determine contact loads in different movements due to its

capability to closely measure these parameters while being non-invasive [30]. In this study, the walking gait was used as the boundary condition for the measurement of the contact loads since this is the most common movement that involves the knee joint. The 6th GCC dataset includes walking loads that were measured using load cells placed on the tibial tray. To obtain a more standard view of the other parameters to be measured, standardized walking knee joint loads were used as boundary conditions, as provided by Bergmann et al. in their study [29]. The generated contact load from these boundary conditions is shown in Figure 3, along with the matched walking load from the dataset.

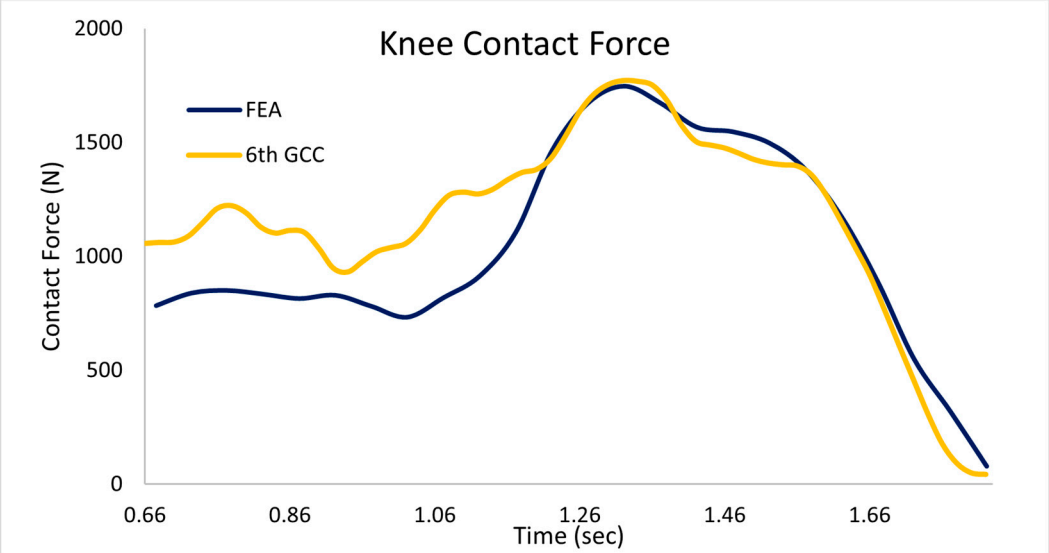

Figure 3. Contact loads from the 6th GCC dataset and FE simulation with boundary conditions from standardized knee loads.

The two distinct peaks of reaction forces are where the peak axial forces occur during the gait cycle. When comparing the peak axial reaction forces between the FEA and the dataset results, it was observed that the disparity was greater along the region of the first peak compared to the second peak. The most probable reason for this is the joint reaction forces during the gait cycle. As seen from Table 2, the differences in knee angles on both peaks were 11 degrees, but peak reaction forces have a different relationship. The first peak axial force was higher than the second for the dataset values which reflected a higher contact force on its first peak compared to the FEA's first peak. Although there were discrepancies present in the contact forces, the trend of this contact force throughout the gait cycle was similar. The percentage errors of the root mean square and standard deviations of both contact force values were 8.84 and 6.69%. This signifies that the standardized knee loads can represent the actual knee loads with minimal errors. This also serves as a validation for the knee joint model.

Table 2. Boundary conditions of the knee at the peak axial forces.

Data Source	Joint Angle		Reaction Force	
	1st Peak	**2nd Peak**	**1st Peak**	**2nd Peak**
6th GCC	33°	72°	2688 N	2118 N
Standardized knee loads [29]	22°	61°	1657 N	1946 N

3.2. Measurement of ACL Graft Tension and Tibial Insert Contact Pressure

Boundary conditions for the overall joint movement were validated by the contact force along the tibiofemoral interface for an implanted knee. But for both the 6th GCC data sets and the standardized knee loads of Bergmann et al., knee implant loads are assumed

to have no ACL. With the presence of an ACL, there is a tension that keeps the femur and the tibia from over-translation. Jagodzinski et al. (2004) measured the tension of the ACL graft at different flexion angles by having a tension load cell attached to the tibial end of the ACL graft [31]. This tension load cell setup was simulated by measuring the reaction forces on the tibial end of the quadruple semitendinosus ACL graft. The simulation gave a descending tension with increasing flexion with values of 47.4, 36.5, 24.25, 5, and 4 N for 0, 10, 20, 30, and 40° of flexion angles. This falls in the range of tension from Jagodzinski et al.'s cadaveric analysis. This provides additional validation for the position of the joint origin as well as the tension provided by the ACL graft on the model.

Due to the additional tension from the ACL graft, contact could also be altered. Shown in Figure 4 are the contact pressure color maps of the original cruciate-retaining tibial insert from the dataset and the ACLR-compatible tibial insert. Here, the contact pressure distribution is shown at the two peak forces. For the first peak axial force, pressure is concentrated on the lateral side of the tibial insert. This happens because, at this part of the walking gait cycle, the weight of the whole body is shifted to the lateral side of the leg as a heel strike occurs. This could be observed in both tibial insert models. The original tibial insert had higher maximum contact pressure compared to the modified tibial insert. As the heel strike movement happens, a prominent load on the knee increases which is the external rotation [32]. The presence of the ACL graft provided more tension to keep the knee joint rotating externally. On the second peak axial force, the body gets ready to shift its weight to the other foot which causes the distribution of the contact pressure on the medial side of the knee. Although there is less external rotation during this stance, the ACL regains tension as extension occurs up to 14° of knee flexion. This tension is more concentrated on bringing the femur and tibia together as it extends rather than preventing external rotation. This ends up having a larger maximum contact pressure when the ACL is present. Although the ACL could have affected these contact pressures, its significance could not be validated due to the lack of sample datasets with which to compare. Despite the lack of significance, the contact pressure was still able to validate the model due to the expected outcomes and in addition to this, the maximum values fell in the accepted range of maximum tibiofemoral interface contact pressures which are about 5 MPa to 20 MPa [18].

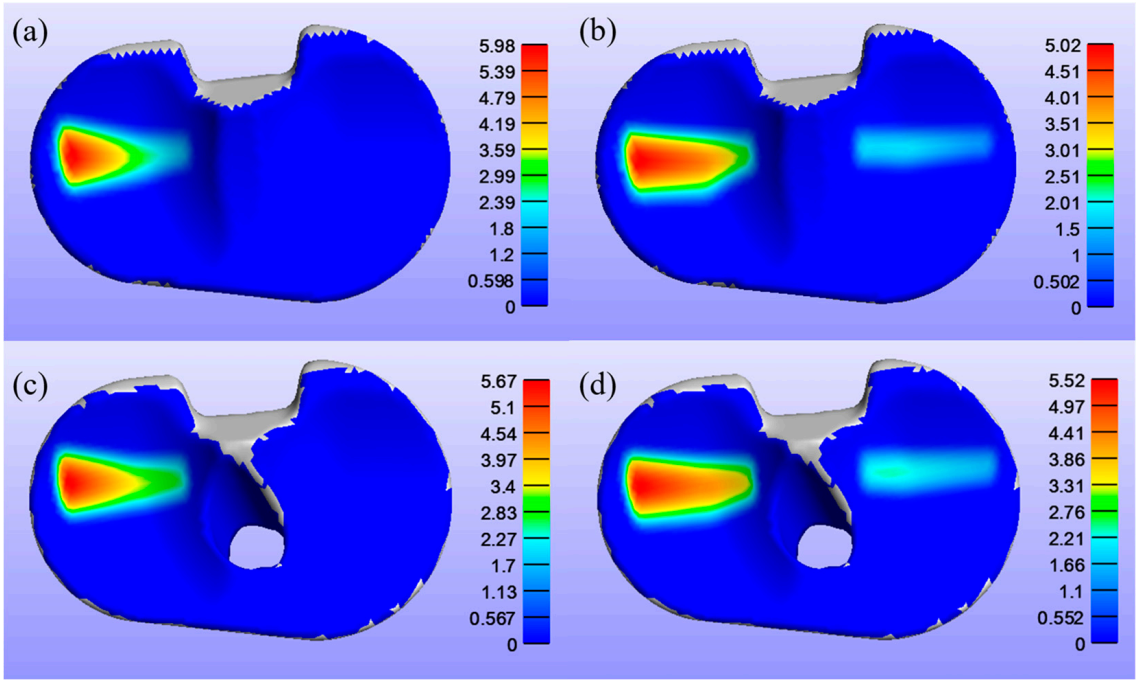

Figure 4. Contact pressure (MPa) distribution on (**a**) original insert at 1st axial peak force, (**b**) original insert at 2nd axial peak force, (**c**) modified insert at 1st axial peak force, and (**d**) modified insert at 2nd axial peak force.

3.3. Comparison of Cortical and Cancellous Bone Graft

The mechanical properties of the bone graft that must hold the ACL in place are important to consider when choosing the material. This will have to be strong enough to hold the stresses that the ACL graft will induce on it at different flexion angles as well as different gait patterns. Bones are known to be brittle materials, which makes mechanical tests an important part of designing the implant. Von Mises stress is one of the most used criteria for evaluating the failure of a material, but this only remains reliable for ductile materials having equal tensile and compressive strength [33]. The Christensen criterion is a better option for testing the failure of brittle materials while still being a reliable metric for ductile materials, and Equation (1) is the main equation taken from Christensen's study [34].

$$\left(\frac{1}{T}-\frac{1}{C}\right)(\sigma_1+\sigma_2+\sigma_3)+\frac{1}{TC}\left[\frac{1}{2}(\sigma_1-\sigma_2)^2+(\sigma_1-\sigma_3)^2+(\sigma_2-\sigma_3)^2\right]\leq 1 \quad (1)$$

In this equation, T and C are the tensile and compressive strengths of the material while σ1, σ2, and σ3 are the principal stresses. This equation will only remain reliable for materials where the compressive strength is greater than the tensile strength, which is the case for the cortical bone as shown in Table 3. The three principal stresses on the cortical bone graft were obtained from the simulation. The tensile principal stresses, which are positive values, were greater than the compressive principal stresses. With the fact that cortical bone compressive strength is greater than the tensile strength and that the tensile principal stresses were greater, failure would most likely occur at regions under tension. Figure 5 shows the safety factor based on the Christensen failure criterion for the cortical bone graft plotted against the percentage of the gait cycle. This showed that the bone graft would not fail at any point of the walking cycle since failure would be reached when the values for this equate to, or exceed, 1.

Table 3. Mechanical strength of bone materials.

Parameters	Cortical	Cancellous/Trabecular
Tensile strength (MPa)	50–151 [35]	138 [36]
Compressive strength (MPa)	130–200 [35]	0.1–16 [35]
Shear strength (MPa)	-	0.05–13 [37]

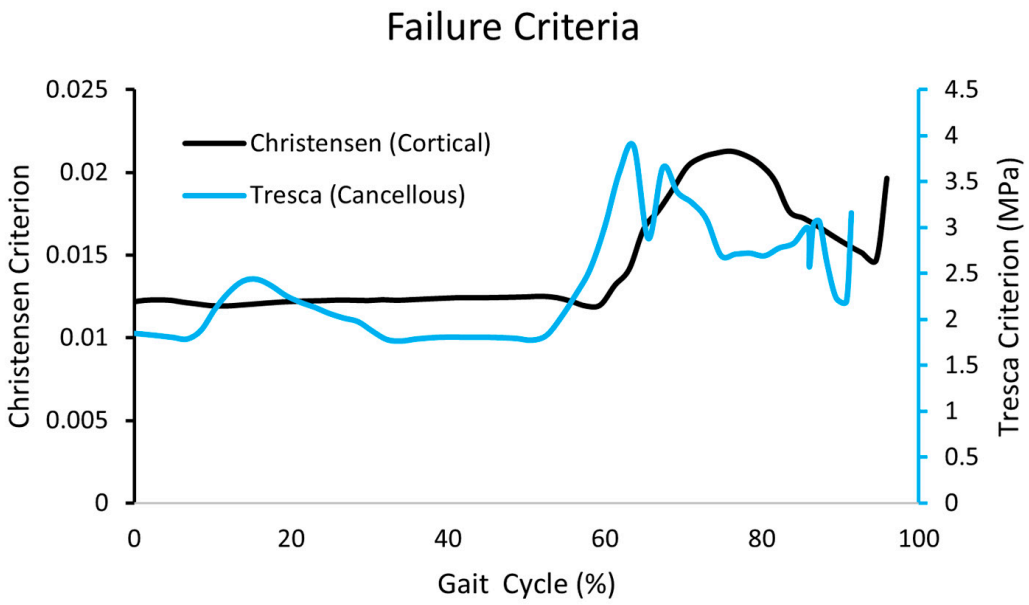

Figure 5. Failure criteria for cortical and cancellous bone grafts.

The problem with Equation (1) is that it is limited to materials having greater compressive strength than tensile strength. Cancellous bone does not fall within this initial condition since its compressive strength is far smaller than its tensile strength. For several failure criteria, materials with larger tensile strength than compressive strength are considered ductile, and there are only a few failure criteria that are reliable for this case. The maximum shear stress criterion or Tresca criterion has been used to test failure on bones and this provides more accurate results compared to normal stress-based criteria because, for ductile materials, failure could occur earlier due to shearing at 45 degrees before the normal stresses reach the tensile or compressive strengths [38,39]. From the FEBio documentation, the maximum shear stress takes the form of Equation (2).

$$\text{Maximum shear stress} = \frac{\sigma_1 - \sigma_3}{2} \tag{2}$$

It can be seen in Figure 5 that the maximum shear stress induced on the cancellous bone graft had a peak value of 3.88 MPa at 63% of the gait cycle. At this shear stress, the cancellous bone graft could fail depending on the bone source since this value is in between the range of the shear strengths reported in the literature [37]. The bone volume fraction of the cancellous bone has been observed to have a non-linear relationship with the shear strength, and samples from the femoral neck were the most likely to have the greatest shear strength [37].

4. Discussion

Finite element analysis has become a powerful tool that gives a cost-effective way of conducting biological research. Different physical phenomena occurring in biological systems can now be studied through simulations that can be achieved with high accuracy depending on controllable parameters. FEA can conduct predictions, visualization, and investigations on the biomechanics of different biological systems while being non-invasive [40]. Computational tools have been used to analyze bypass grafts to optimize blood flow [41]. In orthopedics, it also evaluated an approach to perfecting implant designs before pushing through with the invasive part, which decreases the chances of inducing harm to a test subject. FEA has been used to analyze the failure of different materials for hip implants to optimize the design, which is the same for knee implants [42,43]. Although this tool could be powerful in research, the extent of its accuracy depends on the inputs such as the geometries, mesh quality, boundary conditions, and loads. FEBio Studio is a finite element software that provides tools to generate and analyze biomechanics models [44].

4.1. Standardized Knee Loads and Actual Knee Loads

One of the products that FEA has brought into orthopedics is the development of patient-specific implant designs. This is accomplished by obtaining patient-specific data such as MRI or CT images as well as boundary conditions, and from this, implant designs that would best fit that specific patient. But before conducting the design, sufficient knowledge about a certain implant must be acquired. During this knowledge acquisition, general observation is more beneficial than patient-specific observations to account for the variations between patients and to create a baseline that would be applicable to a wide range of cases. This is where standardized loads become useful. In this study, standard knee loads were used to obtain less patient-specific data and to obtain data for a wider range of knee joint-load conditions. To ensure that the standardized knee loads could still represent the patient-specific loads, where the bone and implant geometries were acquired, the resulting contact forces on the tibiofemoral interface of the FE model were compared with the actual knee contact forces which were provided in the 6th GCC dataset. It is worth noting that the implant geometries such as the tibial tray stem, the tibial insert curvature, and the femoral component curvature were preserved to minimize the modifications that could compromise the results in the validation step. The results show that the standardized knee loads could represent the actual knee loads of the sample patient. Although this

could be representative of actual patient knee loads, this does not guarantee that the results would be accurate for all patients. This only serves as a wider view of the observations to be able to acquire a general idea of what could happen with the design.

4.2. Bone Graft for ACL Graft Tunnel in Total Knee Replacement

The general idea for this knee implant design is to have tibial components that would be compatible with ACL reconstruction, which provides an option to push through with bi-cruciate-retaining total knee replacement when the tibial eminence breaks or the ACL is torn. By having an inner bone graft, the ACL graft is given the chance to reincorporate with the tibia during the healing process, which cannot be achieved if the conventional tibial components are used. In addition to this, the implant serves as a guide on how to position the ACL graft since pre-made tibial tunnels will be present on the bone graft. The process could proceed similar to typical procedures of total knee replacement followed by the procedures in the ACL reconstruction as mentioned in the literature, with additional steps [45,46]. From the preoperative evaluations, the bone graft location and knee implant could be designed. The bone graft with the desired type and dimensions could be harvested and preserved prior to knee replacement. During implantation, the bone graft could be placed after the tibial insert, followed by drilling for the tibial tunnel for the ACL reconstruction. The ACL reconstruction could proceed after the knee replacement with the tibial tunnel ready. With this, the bone graft could heal with the ACL graft. This rough design will provide a general idea of the concept as well as its possible failure.

Cancellous bones or trabecular bones are highly porous and vascularized which improves the rate of healing compared to cortical bone [47]. Due to these properties, mechanical strength is sacrificed. Cancellous bones have relatively low compressive strength compared to cortical bones which makes the former more susceptible to shear yielding. From the predicted stresses in the FE model, cortical bones are far from yielding when subjected to loading during the walking gait cycle, but the cancellous bone could easily yield at the same loading conditions in the orange to cyan region, shown in Figure 6. The choice of a cancellous bone source could impact the success of the bone graft to withstand the ACL graft loads on it. The femoral neck would most likely be the best choice for the source of the cancellous bone graft as it is more likely to have higher shear strength [37]. It would also be important to mention that these results could only occur under walking loads since the study only considers the scenario prior to bone healing.

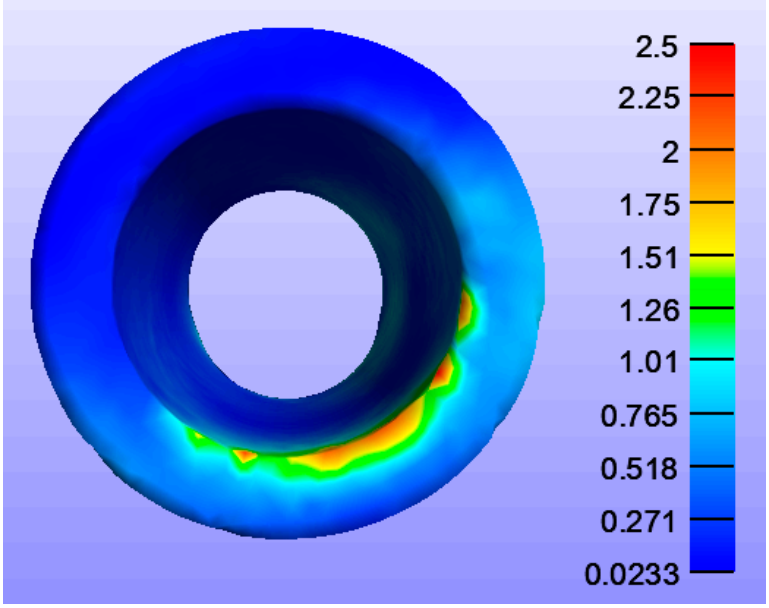

Figure 6. Maximum shear stress (MPa) distribution on the bone graft.

5. Conclusions

In this study, a knee implant design was created to serve as an option for total knee replacement with ACL reconstruction for a bi-cruciate knee arthroplasty which included a bone graft on the tibial components that envelop the ACL graft along the tibial tray and tibial inserts. A knee joint model was created that used standardized knee loads on knee implants with an intact ACL graft. Validation of the use of standardized knee loads was conducted by comparing the contact loads of the model with actual contact loads from the 6th GCC dataset. This validation confirmed that the standardized knee loads can represent the actual knee loads of the source patient without the ACL graft. Additional validation steps were conducted to justify the loading conditions and boundary conditions when an ACL graft was present. The literature data confirmed the reaction forces on the tibial end of the ACL graft at different knee flexion angles. Contact pressures on the tibial insert at the peak axial forces were compared for the model with and without the ACL graft. The values for these were in the typical range of contact pressures at the knee joint, and contact pressure distribution lined up with the proper pressure distribution at the gate cycle percentage where peak axial loads occurred. Lastly, cortical, and cancellous bone materials were compared under their loading conditions during a walking cycle. Christensen failure criterion confirmed that cortical bone can withstand the loading conditions while the maximum shear stress criterion showed that failure could occur for the cancellous bone depending on the material's shear strength, which is affected by the selection of donor site.

Future studies involving this design could study the effectiveness of the bone healing properties of the cancellous bone on both the tibia and the ACL graft. Different gait cycles such as standing up, climbing, and sitting down could be analyzed as well. The strength of the bone graft could also be evaluated at different time points of the rehabilitation since the healed bone could have different material strengths. In addition to this, the geometry of the bone graft could be optimized, such that the stress could be distributed further while still maintaining the knee joint mechanics. The bone graft thickness could also be varied in future studies by using validated knee models for optimization. Nevertheless, this study provides several insights into how computational analysis can augment the expanding research in the field of regenerative medicine and tissue engineering.

Author Contributions: Conceptualization, F.L.F.C. and L.L.T.; methodology, F.L.F.C. and L.L.T.; software, F.L.F.C.; validation, F.L.F.C.; formal analysis, F.L.F.C.; data curation, F.L.F.C.; writing—original draft preparation, F.L.F.C.; writing—review and editing, F.L.F.C. and L.L.T.; visualization, F.L.F.C.; supervision, L.L.T.; funding acquisition, L.L.T. All authors have read and agreed to the published version of the manuscript.

Funding: The publishing of this research was funded by Mapúa University.

Data Availability Statement: The dataset used for the implant geometries, CT data, and knee load data was obtained from the Grand Challenge Competition to Predict In Vivo Knee Loads by SimTK which could be accessed publicly through this link https://simtk.org/projects/kneeloads (accessed on 6 December 2022).

Conflicts of Interest: The authors declare no conflict of interest.

References

1. Anatomy, I.P. Anatomy and physiology, 5. The musculoskeletal system. *Br. J. Healthc. Assist.* **2018**, *12*, 6–9. [CrossRef]
2. Bliven, K.C.H.; Anderson, B.E. Core Stability Training for Injury Prevention. *Sport. Health* **2013**, *5*, 514. [CrossRef]
3. Zhang, L.; Liu, G.; Han, B.; Wang, Z.; Yan, Y.; Ma, J.; Wei, P. Knee Joint Biomechanics in Physiological Conditions and How Pathologies Can Affect It: A Systematic Review. *Appl. Bionics Biomech.* **2020**, *2020*, 7451683. [CrossRef] [PubMed]
4. Vad, V.B.; Adin, D.R.; Osteoarthritis, J.S.K. Knee Osteoarthritis. *Crit. Rev. Phys. Rehabil. Med.* **2022**, *16*, 211–231. [CrossRef]
5. Grässel, S.; Muschter, D. Recent advances in the treatment of osteoarthritis. *F1000Research* **2020**, *9*, 325. [CrossRef]
6. Hsu, H.; Siwiec, R.M. *Knee Arthroplasty*; StatPearls: St. Petersburg, FL, USA, 2022. Available online: https://www.ncbi.nlm.nih.gov/books/NBK507914/ (accessed on 18 April 2023).
7. Dall'Oca, C.; Ricci, M.; Vecchini, E.; Giannini, N.; Lamberti, D.; Tromponi, C.; Magnan, B. Evolution of TKA design. *Acta Bio Med. Atenei Parm.* **2017**, *88*, 17.

8. Marieswaran, M.; Jain, I.; Garg, B.; Sharma, V.; Kalyanasundaram, D. A review on biomechanics of anterior cruciate ligament and materials for reconstruction. *Appl. Bionics Biomech.* **2018**, *2018*, 4657824. [CrossRef]
9. Raines, B.; Naclerio, E.; Sherman, S. Management of Anterior Cruciate Ligament Injury: What's In and What's Out? *Indian J. Orthop.* **2017**, *51*, 563–575. [CrossRef]
10. Kiapour, A.M.; Murray, M.M. Basic science of anterior cruciate ligament injury and repair. *Bone Jt. Res.* **2014**, *3*, 20–31. [CrossRef]
11. Tjoumakaris, F.P.; Herz-Brown, A.L.; Legath-Bowers, A.; Sennett, B.J.; Bernstein, J. Complications In Brief: Anterior Cruciate Ligament Reconstruction. *Clin. Orthop. Relat. Res.* **2012**, *470*, 630. [CrossRef]
12. Smidt, K.P.; Bicknell, R. *Prosthetics in Orthopedics*; StatPearls: St. Petersburg, FL, USA, 2022. Available online: https://www.ncbi.nlm.nih.gov/books/NBK570628/ (accessed on 25 May 2022).
13. Abdelbadie, A.; Toreih, A.A.; Radwan, M.A. ACL status in arthroplasty patients, why not to preserve? *Sicot-J* **2018**, *4*, 1. [CrossRef]
14. Pritchett, J.W. Bicruciate Total Knee Replacement. In *Personalized Hip and Knee Joint Replacement*; Springer: Cham, Switzerland, 2020; pp. 265–275. [CrossRef]
15. Archunan, M.W.; Petronis, S. Bone Grafts in Trauma and Orthopaedics. *Cureus* **2021**, *13*, e17705. [CrossRef]
16. Roberts, T.T.; Rosenbaum, A.J. Bone grafts, bone substitutes and orthobiologics. *Organogenesis* **2012**, *8*, 114–124. [CrossRef]
17. Haghani, R. Finite element modelling of adhesive bonds joining fibre-reinforced polymer (FRP) composites to steel. In *Rehabilitation of Metallic Civil Infrastructure Using Fiber Reinforced Polymer (FRP) Composites Types Properties and Testing Methods*; Woodhead Publishing: Sawston, UK, 2014; pp. 60–95. [CrossRef]
18. Loi, I.; Stanev, D.; Moustakas, K. Total Knee Replacement: Subject-Specific Modeling, Finite Element Analysis, and Evaluation of Dynamic Activities. *Front. Bioeng. Biotechnol.* **2021**, *9*, 648356. [CrossRef]
19. Fregly, B.J.; Besier, T.F.; Lloyd, D.G.; Delp, S.L.; Banks, S.A.; Pandy, M.G.; D'Lima, D.D. Grand challenge competition to predict in vivo knee loads. *J. Orthop. Res.* **2012**, *30*, 503–513. [CrossRef] [PubMed]
20. Fedorov, A.; Beichel, R.; Kalpathy-Cramer, J.; Finet, J.; Fillion-Robin, J.C.; Pujol, S.; Bauer, C.; Jennings, D.; Fennessy, F.; Sonka, M.; et al. 3D Slicer as an image computing platform for the Quantitative Imaging Network. *Magn. Reson. Imaging* **2012**, *30*, 1323–1341. [CrossRef] [PubMed]
21. Shino, K.; Mae, T.; Tachibana, Y. Anatomic ACL reconstruction: Rectangular tunnel/bone–patellar tendon–bone or triple-bundle/semitendinosus tendon grafting. *J. Orthop. Sci.* **2015**, *20*, 457–468. [CrossRef]
22. Nema, S.K.; Balaji, G.; Akkilagunta, S.; Menon, J.; Poduval, M.; Patro, D. Radiologic assessment of femoral and tibial tunnel placement based on anatomic landmarks in arthroscopic single bundle anterior cruciate ligament reconstruction. *Indian J. Orthop.* **2017**, *51*, 286–291. [CrossRef] [PubMed]
23. Yin, L.; Chen, K.; Guo, L.; Cheng, L.; Wang, F.; Yang, L. Identifying the Functional Flexion-extension Axis of the Knee: An In-Vivo Kinematics Study. *PLoS ONE* **2015**, *10*, e0128877. [CrossRef]
24. Fritsch, B.; Figueroa, F.; Semay, B. Graft Preparation Technique to Optimize Hamstring Graft Diameter for Anterior Cruciate Ligament Reconstruction. *Arthrosc. Tech.* **2017**, *6*, e2169–e2175. [CrossRef]
25. Tran, T.D.; Tran, Q.L. A cadaveric study on the anatomy of anterior cruciate ligament in Vietnamese adults. *Asia-Pac. J. Sport. Med. Arthrosc. Rehabil. Technol.* **2018**, *14*, 22–25. [CrossRef]
26. Benos, L.; Stanev, D.; Spyrou, L.; Moustakas, K.; Tsaopoulos, D.E. A Review on Finite Element Modeling and Simulation of the Anterior Cruciate Ligament Reconstruction. *Front. Bioeng. Biotechnol.* **2020**, *8*, 967. [CrossRef] [PubMed]
27. Liu, F.; Zhang, D.Z.; Zhang, P.; Zhao, M.; Jafar, S. Mechanical properties of optimized diamond lattice structure for bone scaffolds fabricated via selective laser melting. *Materials* **2018**, *11*, 374. [CrossRef] [PubMed]
28. Khaniki, H.B.; Ghayesh, M.H.; Chin, R.; Amabili, M. Hyperelastic structures: A review on the mechanics and biomechanics. *Int. J. Non-Linear Mech.* **2023**, *148*, 104275. [CrossRef]
29. Bergmann, G.; Bender, A.; Graichen, F.; Dymke, J.; Rohlmann, A.; Trepczynski, A.; Heller, M.O.; Kutzner, I. Standardized Loads Acting in Knee Implants. *PLoS ONE* **2014**, *9*, e86035. [CrossRef]
30. Cassiolas, G.; Di Paolo, S.; Marchiori, G.; Grassi, A.; Della Villa, F.; Bragonzoni, L.; Visani, A.; Giavaresi, G.; Fini, M.; Zaffagnini, S.; et al. Knee Joint Contact Forces during High-Risk Dynamic Tasks: 90° Change of Direction and Deceleration Movements. *Bioengineering* **2023**, *10*, 179. [CrossRef]
31. Jagodzinski, M.; Foerstemann, T.; Mall, G.; Krettek, C.; Bosch, U.; Paessler, H. Analysis of forces of ACL reconstructions at the tunnel entrance: Is tunnel enlargement a biomechanical problem? *J. Biomech.* **2005**, *38*, 23–31. [CrossRef]
32. Aali, S.; Rezazadeh, F.; Badicu, G.; Grosz, W.R. Effect of Heel-First Strike Gait on Knee and Ankle Mechanics. *Medicina* **2021**, *57*, 657. [CrossRef]
33. Pérez-González, A.; Iserte-Vilar, J.L.; González-Lluch, C. Interpreting finite element results for brittle materials in endodontic restorations. *Biomed. Eng. Online* **2011**, *10*, 44. [CrossRef]
34. Christensen, R.M. A comparative evaluation of three isotropic, two property failure theories. *J. Appl. Mech.* **2006**, *73*, 852–859. [CrossRef]
35. Gerhardt, L.-C.; Boccaccini, A.R. Review–Bioactive Glass and Glass-Ceramic Scaffolds for Bone Tissue Engineering. *Materials* **2010**, *3*, 3867–3910. [PubMed]
36. Smotrova, E.; Li, S.; Tashkinov, M.; Shalimov, A.; Silberschmidt, V.V. Failure behaviour of human trabecular bone. *Procedia Struct. Integr.* **2021**, *37*, 257–262. [CrossRef]

37. Sanyal, A.; Gupta, A.; Bayraktar, H.H.; Kwon, R.Y.; Keaveny, T.M. Shear strength behavior of human trabecular bone. *J. Biomech.* **2012**, *45*, 2513–2519. [CrossRef] [PubMed]
38. Oftadeh, R.; Perez-Viloria, M.; Villa-Camacho, J.C.; Vaziri, A.; Nazarian, A. Biomechanics and Mechanobiology of Trabecular Bone: A Review. *J. Biomech. Eng.* **2015**, *137*, 010802. [CrossRef]
39. Stewart, M. Engineering Principles. In *Surface Production Operations*; Elsevier: Amsterdam, The Netherlands, 2021; pp. 1–17. [CrossRef]
40. Trivedi, S. Finite element analysis: A boon to dentistry. *J. Oral Biol. Craniofacial Res.* **2014**, *4*, 200–203. [CrossRef] [PubMed]
41. Apan, J.J.; Tayo, L.; Honra, J. Numerical Investigation of the Relationship between Anastomosis Angle and Hemodynamics in Ridged Spiral Flow Bypass Grafts. *Appl. Sci.* **2023**, *13*, 4046. [CrossRef]
42. Colic, K.; Sedmak, A.; Grbovic, A.; Tatic, U.; Sedmak, S.; Djordjevic, B. Finite Element Modeling of Hip Implant Static Loading. *Procedia Eng.* **2016**, *149*, 257–262. [CrossRef]
43. Kohli, A.; Mathad, M.; Hosamani, S.V.; Adagimath, M.K.; Kotturshettar, B.B. Finite element analysis of knee joint implant for varying bio material using ANSYS. *Mater. Today Proc.* **2022**, *59*, 941–950. [CrossRef]
44. Maas, S.A.; Ellis, B.J.; Ateshian, G.A.; Weiss, J.A. FEBio: Finite Elements for Biomechanics. *J. Biomech. Eng.* **2012**, *134*, 011005. [CrossRef]
45. DiFelice, G.S.; Villegas, C.; Taylor, S. Anterior Cruciate Ligament Preservation: Early Results of a Novel Arthroscopic Technique for Suture Anchor Primary Anterior Cruciate Ligament Repair. *Arthrosc. J. Arthrosc. Relat. Surg.* **2015**, *31*, 2162–2171. [CrossRef]
46. Patrick, W.; Shady, E.M.; Christoph, T.; Ramin, K.; Xaver, F. Advanced Anterior Cruciate Ligament Repair and Reconstruction Techniques for Different Rupture Types. *Arthrosc. Tech.* **2020**, *9*, e969. [CrossRef] [PubMed]
47. Voss, K.; Montavon, P.M. Fractures. In *Feline Orthopedic Surgery and Musculoskeletal Disease*; Elsevier: Amsterdam, The Netherlands, 2009; pp. 129–152. [CrossRef]

Disclaimer/Publisher's Note: The statements, opinions and data contained in all publications are solely those of the individual author(s) and contributor(s) and not of MDPI and/or the editor(s). MDPI and/or the editor(s) disclaim responsibility for any injury to people or property resulting from any ideas, methods, instructions or products referred to in the content.